A synergy between mechanosensitive calcium- and membrane-binding mediates tension-sensing by C2-like domains

Zhouyang Shen[a,b], Kalina T. Belcheva[c], Mark Jelcic[a,b,1], King Lam Hui[a], Anushka Katikaneni[a,2], and Philipp Niethammer[a,3]

[a]Cell Biology Program, Memorial Sloan Kettering Cancer Center, New York, NY 10065; [b]Gerstner Sloan Kettering Graduate School of Biomedical Sciences, New York, NY 10065; and [c]Biochemistry, Cellular and Molecular Biology Allied Program, Weill Cornell Graduate School of Medical Sciences, New York, NY 10065

When nuclear membranes are stretched, the peripheral membrane enzyme cytosolic phospholipase A2 (cPLA₂) binds via its calcium-dependent C2 domain (cPLA₂-C2) and initiates bioactive lipid signaling and tissue inflammation. More than 150 C2-like domains are encoded in vertebrate genomes. How many of them are mechanosensors and quantitative relationships between tension and membrane recruitment remain unexplored, leaving a knowledge gap in the mechanotransduction field. In this study, we imaged the mechanosensitive adsorption of cPLA₂ and its C2 domain to nuclear membranes and artificial lipid bilayers, comparing it to related C2-like motifs. Stretch increased the Ca^{2+} sensitivity of all tested domains, promoting half-maximal binding of cPLA₂ at cytoplasmic resting-Ca^{2+} concentrations. cPLA₂-C2 bound up to 50 times tighter to stretched than to unstretched membranes. Our data suggest that a synergy of mechanosensitive Ca^{2+} interactions and deep, hydrophobic membrane insertion enables cPLA₂-C2 to detect stretched membranes with antibody-like affinity, providing a quantitative basis for understanding mechanotransduction by C2-like domains.

mechanotransduction | membrane | nucleus | cPLA2 | calcium

Eicosanoids are powerful bioactive lipids generated by the enzymatic oxidation of the polyunsaturated fatty acid arachidonic acid (AA). Among other functions (1), eicosanoids participate in mechanotransduction, for example, during bone load sensing in mammals and osmotic wound detection in zebrafish (2, 3). The rate-limiting step of eicosanoid synthesis is the cleavage of AA from nuclear and endoplasmic reticulum (ER) membranes by the inflammatory lipid hydrolase cPLA₂. Recently, this enzyme emerged as a nuclear membrane (NM) mechanosensor that detects cell swelling and confinement (2, 4–6). Together with Ca^{2+}, NM-stretch promotes the bilayer adsorption of cPLA₂ via its C2-domain, which allows the enzyme to hydrolyze AA from phospholipids. Lipoxygenases (ALOX5, ALOX12, etc.), cyclooxygenases (PTGS1 and PTGS2), and other enzymes convert AA into the eicosanoids, which include the leukotrienes, prostaglandins, and other bioactive lipids.

There are more than 150 vertebrate proteins with C2-like domains, which include both classic C2 domains, such as those in protein kinase C (PKC) and cPLA₂, as well as the structurally related PLAT (Polycystin-1, Lipoxygenase, Alpha-Toxin) domain as in ALOX5 and ALOX12. Classic C2 domains form a β-sandwich composed of eight β-strands, whereas PLAT domains form a β-sandwich composed of two β-sheets and four β-strands. The mechanosensitivity of these Ca^{2+}-dependent membrane-interaction motifs has not been systematically investigated. Therefore, it is currently difficult to predict which C2-like domains act as membrane tension sensors and what the distinguishing features of mechanosensitive C2-like domains are. To gain quantitative insights into this, we decided to focus on a representative group of two classical C2-domains and two PLAT domains, namely, *dr* cPla₂-C2 and *hs* cPLA₂-C2 (*Danio rerio* and *Homo sapiens*), *hs* PKCγ-C2 (*H. sapiens*), *dr* Alox5a-PLAT (*D. rerio*), and *dr* Alox12-PLAT (*D. rerio*).

cPLA₂-C2's calcium-binding loops (CBRs) contain Ca^{2+}-binding residues and two clusters of exposed hydrophobic amino acids that promote membrane-binding and penetration. The Ca^{2+} ions neutralize negative surface charges of lipid headgroups, whereas CBR1 and CBR3 deeply insert into the lipid bilayer and interact with lipid hydrocarbons (7–11). Like cPLA₂-C2, ALOX5-PLAT binds to zwitterionic membranes via hydrophobic membrane insertion and electrostatic interactions (11, 12), whereas the binding mechanism of ALOX12-PLAT is less clear. PKCγ-C2 binds phosphatidylserine (PS)-rich membranes primarily via electrostatic interactions (13). Electron paramagnetic resonance and molecular dynamics studies of the related PKCα-C2 domain underline that compared to cPLA₂-C2, PKCs interact more shallowly with membranes (7, 14, 15).

Significance

A cell must be able to measure whether the lipid membranes that surround its insides are stretched. Currently, mechanosensitive ion channels are the best-studied class of membrane tension sensors, but recent work suggests that peripheral membrane enzymes that gauge nuclear confinement or swelling during cell migration or upon tissue injury constitute a second class. The mechanosensitivity of these enzymes derives from their calcium-dependent ("C2-like") membrane-interaction domains. Although these can be found in many important signaling proteins, they have remained virtually unstudied as mechanotransducers. How membrane tension controls these domains and what features render them mechanosensitive is unclear. Here, we show that membrane tension-sensing by C2-like domains is mediated by a synergy between mechanosensitive calcium-binding and membrane insertion.

Here, we purified the fluorescent protein fusions of these domains from bacteria and analyzed their adsorption to stretched and unstretched artificial bilayers at different Ca^{2+}- and C2-like domain concentrations. As an artificial membrane system, we chose giant unilamellar vesicles (GUVs) generated by a nylon net hydration technique. GUV bilayers are basically flat and thus represent much better the topology of large cell organelles (e.g., the nucleus) than the highly curved, small unilamellar vesicles (SUVs, <100 nm) often used for spectroscopic measurements of membrane–protein interactions. Osmotic swelling enabled the confocal imaging of stretch-dependent domain adsorption to many GUVs in parallel (i.e., under the same conditions), which is hard to achieve via one-by-one stretching methods (e.g., micropipette). The resultant robustness of our assay allowed us to define distinguishing features of mechanosensitive C2-like domains.

Results

Membrane Tension Increases the Ca^{2+} Sensitivity of C2-Like Domains. GUVs were produced either by drying lipid films on nylon nets and hydrating them with a 0.5 M sucrose solution (*SI Appendix*, Fig. S1*A*) or by standard electroformation (16). To this end, we used binary lipid mixtures of zwitterionic dipalmitoyl-phosphatidylcholine (DPPC) with or without 16% or 26% brain-derived PS or mixtures of dioleoyl-phosphatidylcholine (DOPC) with or without 18% conical dioleoyl glycerol (DOG) to vary bilayer-charge and -packing density through the inclusion of anionic and differently shaped lipids. Our nylon net method markedly increased the homogeneity and yield of unilamellar vesicles (median radius ~7 μm) compared to a standard gentle hydration protocol (*SI Appendix*, Fig. S1 *B* and *C*). We suppose that the advantageous wetting properties of nylon nets support a particularly thin lipid film distribution, thereby increasing the likelihood of unilamellar structures during hydration.

To osmotically stretch multiple GUVs at the same time, we exposed them to a hypotonic buffer, and measured domain adsorption by confocal fluorescence microscopy followed by automated image recognition and processing (*Methods*). After all visible surface invaginations had disappeared and the GUVs had reached maximal circularity, we observed domain-binding (Fig. 1*A* and Movie S1). As expected, mutation of Ca^{2+}-binding residues completely abrogated the membrane interactions of the cPla2-C2-eGFP fusion protein (*SI Appendix*, Fig. S2 *C* and *D*).

Eventually, the GUVs ruptured, which caused a sudden decrease in light refraction due to sucrose leakage, a decrease in vesicle diameter, and a loss of domain fluorescence from the GUV rim (Fig. 1 *B* and *C*, *SI Appendix*, Figs. S3 and S4*A*, and Movies S2, S3, and S4). To confirm the direct correlation of osmotic swelling and membrane tension in our GUV assay, we used the fluorescent lipid tension reporter Flipper-TR (17) that measures membrane tension by changes in fluorescence lifetime. GUVs in hypotonic buffer exhibited increased Flipper-TR fluorescence lifetimes compared to isotonic buffer, consistent with their expected, higher-membrane tension (*SI Appendix*, Fig. S4*B*). GUV rupture led to a sudden drop of Flipper-TR fluorescence lifetime indicative of membrane relaxation (*SI Appendix*, Fig. S4*C*).

Without any GUV stretch ($\Delta M_{OSM} = 0$ mOsm), Ca^{2+}-dependent domain adsorption was often too low for reliable curve fitting. As a result, we quantitatively compared the $[Ca^{2+}]$-versus-adsorption isotherms of weakly ($\Delta M_{OSM} = 100$ mOsm; Fig. 1*D* and *SI Appendix*, Fig. S5, dashed lines) and strongly stretched GUVs ($\Delta M_{OSM} = 240$ mOsm; Fig. 1*D* and *SI Appendix*, Fig. S5, solid lines) by fitting a Hill equation. GUV tension lowered the Ca^{2+} concentration required for

half-maximal domain-binding ($[Ca^{2+}]_{1/2}$). We conclude that mechanosensitive Ca^{2+} interactions are a common feature of C2-like domains. In part, they may result from the coupled-binding equilibria of domain-Ca^{2+}- and domain–membrane interactions. Namely, the increase in membrane affinity (that occurs when stretching lowers the thermodynamic cost of membrane insertion) should trigger a simultaneous increase in the Ca^{2+} affinity of the domain–membrane complex. In addition, membrane stretch may facilitate Ca^{2+} adsorption to lipid bilayers (18), as previously observed for membrane curvature (19).

Tension Increases the Membrane Affinity of Some C2-Like Motifs. To determine the effect of stretch on the maximal adsorption and apparent membrane affinity of C2-like domains, we varied domain concentration at low (i.e., $[Ca^{2+}] = 20$ μM; Fig. 1 *E* and *F*, open bars; *SI Appendix*, Fig. S6)- or high-Ca^{2+} concentrations (i.e., $[Ca^{2+}] = 200$ to 500 μM; Fig. 1 *E* and *F*, gray bars; *SI Appendix*, Fig. S6) in the absence ($\Delta M_{OSM} = 0$ mOsm, Fig. 1 *E* and *F* and *SI Appendix*, Fig. S6, dashed lines) or presence ($\Delta M_{OSM} = 240$ mOsm, Fig. 1 *E* and *F* and *SI Appendix*, Fig. S6, solid lines) of membrane stretch. These two $[Ca^{2+}]$ regimes were picked to roughly match the $[Ca^{2+}]_{1/2}$ of the domains. For better quantitative comparison, we fitted the adsorption versus [Domain] curves with a Langmuir equation. Osmotic stretch and conical lipids increased the membrane adsorption capacity B_{max} for all tested C2-like domains (*SI Appendix*, Fig. S6*B*, *Upper*), except for *hs* cPLA2-C2 in which the uncertainty of B_{max} under isotonic, unstretched conditions was too large to allow this conclusion. C2-like domains partially insert into the membrane, regardless of whether they hydrophobically interact with its acyl-chain core, such as cPLA2-C2 or ALOX5-PLAT, or merely shallowly attach via Ca^{2+} and electrostatics, such as PKCγ-C2. Pulling lipid headgroups apart by stretch makes space for partial insertion, which increases the number of potential adsorption sites and with it, B_{max}. Accordingly, incorporation of lipids known to loosen lipid-packing because of their small headgroups or kinked fatty acid side chains (DOG or DOPC) raised B_{max} even in the absence of membrane tension (*SI Appendix*, Fig. S6; compare adsorption at $\Delta M_{OSM} = 0$ mOsm between DPPC, DOPC, and DOPC/DOG vesicles).

Interestingly, stretch differentially affected the apparent domain affinity (K_d') to these adsorption sites: With Ca^{2+} provided in excess (200 to 500 μM), stretch tightened membrane-binding only for cPla2-C2 and Alox5a-PLAT, whereas it did not affect or even weakened binding for Alox12-PLAT and PKCγ-C2, respectively (Fig. 1*F*). Importantly, this selective mechanosensitive effect correlates with the ability of these domains to hydrophobically interact with the membrane acyl-core: cPLA2-C2, whose bilayer interactions are dominated by hydrophobic insertion into the membrane, tightened its membrane-binding most drastically upon stretch. In line with the conservation of critical hydrophobic residues in the CBRs of *dr* and *hs* cPLA2-C2 (*SI Appendix*, Fig. S2 *A* and *B*), the membrane affinities of both domains were very sensitive to membrane stretch (*SI Appendix*, Fig. S6*B*, *Bottom*). By contrast, PKCγ-C2, whose membrane association is dominated by electrostatics, showed the opposite effect. A "C2-unlike" PH domain (AKT1) showed no considerable mechanosensitivity to osmotic membrane stretch or rupture (*SI Appendix*, Fig. S7). Hence, stretch-sensing does not seem to be a universal feature of C2-like and other membrane-binding motifs.

The stretch-induced affinity changes depended on lipid composition: On DPPC/PS and DOPC GUVs, stretch strengthened the membrane interactions of cPla2-C2 by up to 50 times. For DOPC/DOG and DPPC GUVs, much-lower affinity changes were observed (approximately two to four times). To directly test the role of hydrophobic interactions for cPla2-C2's mechanosensitivity, we mutated two pairs of conserved, hydrophobic
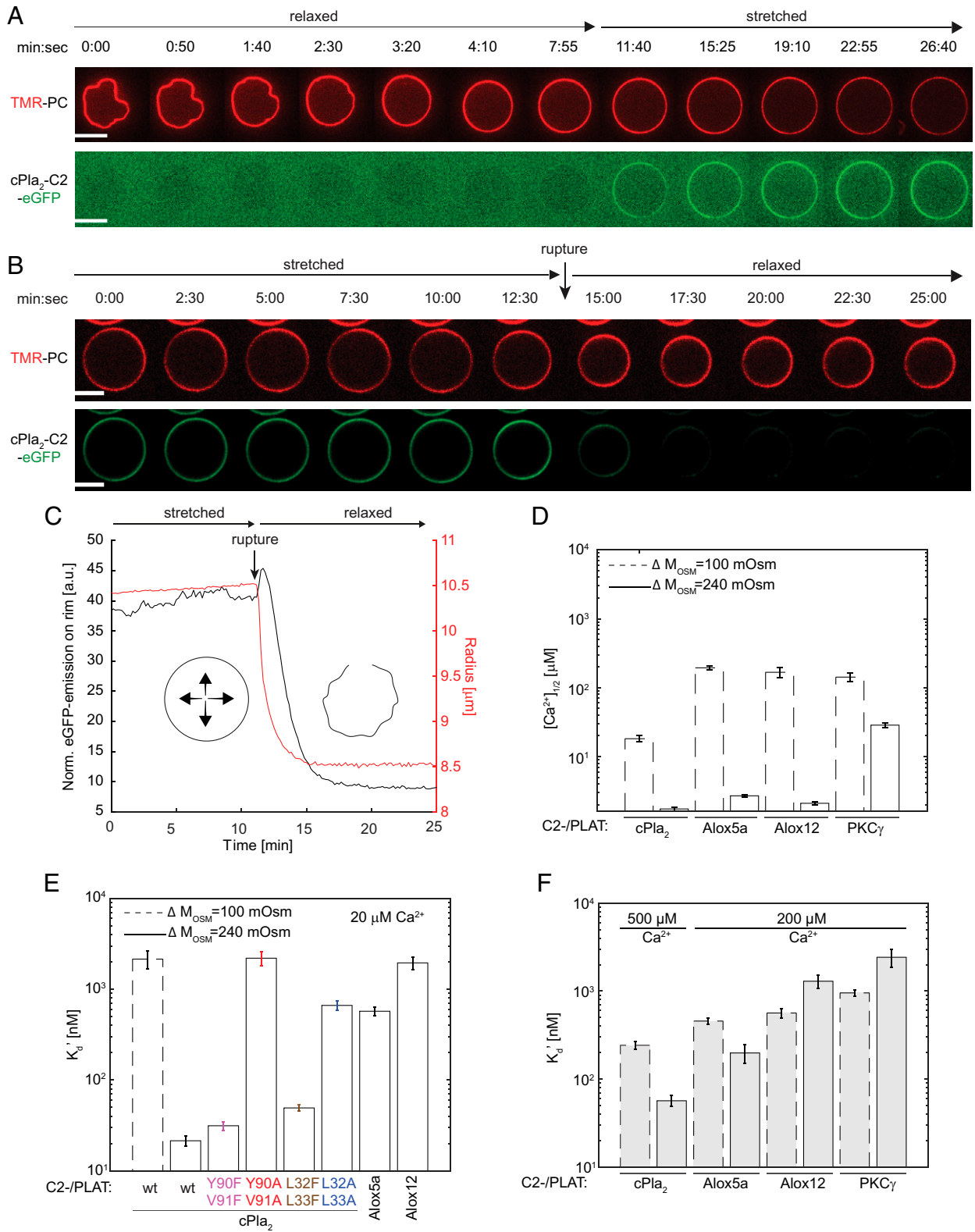
Fig. 1. Probing the mechanosensitivity of C2-like domains with GUVs. (*A*) Representative time-lapse montage of *dr* cPla$_2$-C2-eGFP adsorption to GUVs after transferring GUVs (DPPC+16% Brain PS) from hypertonic (ΔM_{OSM} = −400 mOsm) to hypotonic (ΔM_{OSM} = 240 mOsm) solution. (Scale bars, 10 μm.) (Movie S1) (*B*) Representative time-lapse montage of *dr* cPla$_2$-C2-eGFP desorption from a ruptured GUV (DPPC+16% Brain PS). TMR PC, TopFluor TMR labeled phosphatidylcholine (Scale bars, 10 μm.) (Movie S2). (*C*) Quantification of the experiment depicted in *B*. (*D*) Ca^{2+} concentrations required for half-maximal equilibrium binding of the indicated domains to GUVs exposed to low (dashed lines) or high (solid lines) osmotic stretch (*SI Appendix*, Fig. S5). (*E* and *F*) Apparent membrane-binding affinity (K$_d$′) on unstretched (dashed lines) and stretched (solid lines) GUVs at low [Ca^{2+}] (20 μM) (*E*) or high [Ca^{2+}] (200 to 500 μM) (*F*) (*SI Appendix*, Fig. S6). Error bars, 95% CI of Hill or Langmuir equation-fitting through isotherm data consisting of n > 300 individual GUV measurements across nine different Ca^{2+}- (Hill fit) or domain concentrations (Langmuir fit). GUV lipid composition: 74% DPPC + 26% Brain PS for PKCγ-C2 and 84% DPPC + 16% Brain PS for all other domains. For sample sizes, refer to Dataset S2A.

Shen et al.
A synergy between mechanosensitive calcium- and membrane-binding
mediates tension-sensing by C2-like domains

PNAS | 3 of 9
https://doi.org/10.1073/pnas.2112390119

residues known to participate in membrane penetration. Indeed, both L32A/L33A and Y90A/V91A double mutants showed severely reduced stretch-sensing, whereas the corresponding conservative L32F/L33F and Y90F/V91F double mutants did not (Fig. 1E and *SI Appendix*, Fig. S6).

Tension and Curvature Sensors Recognize the Same Membrane Sites. The concept that hydrophobic protein insertion measures internal membrane stresses has been mostly studied in the context of membrane curvature-sensing by amphipathic lipid-packing sensor (ALPS) motifs (20–24). ARFGAP1, a regulator of vesicle-trafficking, contains tandem ALPS motifs (ARF-GAP1-ALPS, *SI Appendix*, Fig. S1D). If curvature- and stretch-sensing occurs through the same structural membrane intermediates, ARFGAP1-ALPS should be a tension sensor and compete with cPla$_2$-C2 for the same adsorption sites. Indeed, ARFGAP1-ALPS showed preferential adsorption to stretched and desorption from ruptured GUVs (*SI Appendix*, Fig. S8 and Movie S5). Furthermore, prebound cPla$_2$-C2 blocked ARFGAP1-ALPS adsorption to GUVs (Fig. 2A and Movie S6). Prebound ARFGAP1-ALPS was displaced from stretched GUVs only in the presence but not absence of cPla$_2$-C2 (Fig. 2B and *SI Appendix*, Fig. S8C and Movies S7 and S8). When prebound cPla$_2$-C2 desorbed due to Ca^{2+} removal, ARFGAP1-ALPS started to bind (Fig. 2C and Movie S9). Altogether, these data argue that stretch and curvature sensors compete for the same adsorption sites, namely, lipid-packing defects. This finding is consistent with a preprint showing increased ARFGAP1-ALPS adsorption to GUVs upon micropipette aspiration (25), together with a recently published study demonstrating curvature-sensitivity of cPLA$_2$-C2 (26). Although ARFGAP1-ALPS can sense membrane stretch independent of Ca^{2+}, its moderate stretch-sensitivity compared to cPLA$_2$-C2 (*SI Appendix*, Fig. S8A) leaves whether it acts as a membrane tension sensor in vivo uncertain.

NM-Tension Promotes cPLA$_2$ Adsorption at Resting [Ca^{2+}]. To test whether the insights from our reconstitution experiments hold up in a more physiologically complex situation, we sought to determine the binding kinetics of full-length cPLA$_2$ to stretched and unstretched, intact nuclei. Whereas it is hard to vary cellular protein concentrations precisely enough to generate reliable Langmuir isotherms, adjusting Ca^{2+} concentrations together with NM-stretch is feasible. To this end, we took advantage of a previously established experimental setup (4): Using low-dose digitonin, we permeabilized the plasma membrane of A549 and HeLa cells (4) expressing fluorescent zebrafish cPla$_2$ (cPla$_2$-mKate2), leaving the cell nuclei visibly intact. [Ca^{2+}] and NM-stretch were adjusted by varying the concentrations of calcium chloride and high–molecular weight polyvinylpyrrolidone (PVP) in the cell lysis buffer (Fig. 3A). Lowering extranuclear [PVP] caused colloid osmotic swelling of the nucleus and cPla$_2$ adsorption to the inner NM as a function of osmotic stretch (Fig. 3B). Intriguingly, membrane tension diminished the Ca^{2+} concentration required for half-maximal adsorption from [Ca^{2+}]$_{1/2}$ ~1.6 μM (low NM-stretch) to [Ca^{2+}]$_{1/2}$ ~60 nM (high NM-stretch) (Fig. 3C). In HeLa cells, Ca^{2+}-sensitivity increased from [Ca^{2+}]$_{1/2}$ ~250 nM (low NM-stretch) to ~90 nM (high NM-stretch) (*SI Appendix*, Fig. S9). The different baseline-binding of cPla$_2$ to the osmotically unstretched inner NM of A549 and HeLa cells might reflect different conical lipid concentrations or different baseline NM-tension in these cells. Considering the different assay conditions, these nanomolar [Ca^{2+}]$_{1/2}$ values agree remarkably well with the available literature: The [Ca^{2+}] required for half-maximal activity of Ca^{2+}-dependent PLA$_2$ (i.e., likely cPLA$_2$) in the sonicated particulate fraction of homogenized macrophages ranges around 100 to 200 nM (27). This is not too far off from the 60 to 90 nM measured by us for cPla$_2$ adsorption to stretched NMs. By contrast, the [Ca^{2+}]$_{1/2}$ values for the recruitment of recombinant cPLA$_2$-C2 to stretched GUVs ([Ca^{2+}]$_{1/2}$ ~1.2 to 1.7 μM; Fig. 1D and Dataset S1) or unstretched SUVs ([Ca^{2+}]$_{1/2}$ =3.3 ± 0.4 μM) (28) are substantially
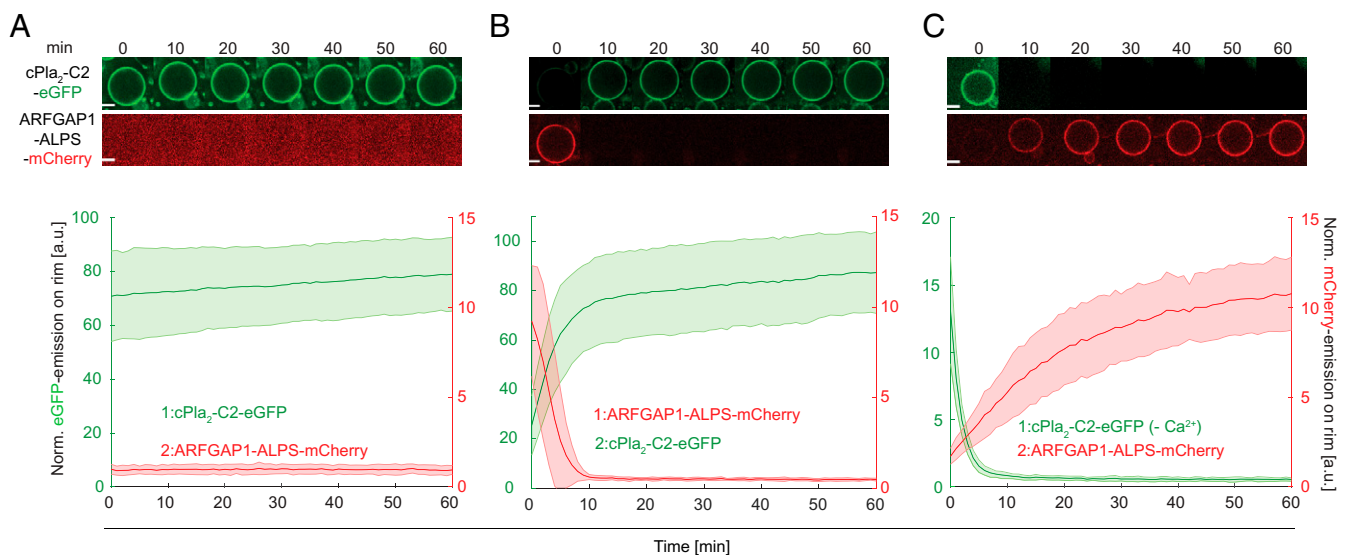

Fig. 2. cPla$_2$-C2 displaces the curvature sensor ARFGAP1-ALPS from stretched GUVs. (A, *Top*) Representative time-lapse montage of domain–membrane interactions after transferring GUVs with prebound *dr* cPla$_2$-C2-eGFP to hypotonic solution (ΔM$_{OSM}$ = 240 mOsm) supplemented with *hs* ARFGAP1-ALPS-mCherry (Movie S6). (*Bottom*) Quantification of normalized mean GUV rim fluorescence of ARFGAP1-ALPS-mCherry (n = 55 GUVs) and cPla$_2$-C2-eGFP (n = 29 GUVs). [Ca^{2+}] = 20 μM. (B, *Top*) Representative time-lapse montage of domain–membrane interactions after transferring GUVs with prebound ARFGAP1-ALPS-mCherry to hypotonic solution (ΔM$_{OSM}$ = 240 mOsm) supplemented with cPla$_2$-C2-eGFP. Note, ARFGAP1-ALPS-mCherry desorption was not observed in the absence of cPla$_2$-C2-eGFP (*SI Appendix*, Fig. S8C and Movies S7 and S8). (*Bottom*) Quantification of mean normalized GUV rim fluorescence of ARFGAP1-ALPS-mCherry (n = 18 GUVs) and cPla$_2$-C2-eGFP (n = 22 GUVs). [Ca^{2+}] = 20 μM. (C, *Top*) Representative time-lapse montage of domain–membrane interactions after transferring GUVs with prebound cPla$_2$-C2-eGFP to Ca^{2+}-depleted solution (ΔM$_{OSM}$ =240 mOsm) supplemented with ARFGAP1-ALPS-mCherry(Movie S9). (*Bottom*) Quantification of mean fluorescence of ARFGAP1-ALPS-mCherry (n =14 GUVs) and cPla$_2$-C2-eGFP (n =22 GUVs) on GUV membranes. [Ca^{2+}] = 20 to 0 μM. (All subfigures: Scale bars, 10 μm.) Shaded error, SD. GUV lipid composition: 100% DPPC. For sample sizes, refer to Dataset S2B.

higher. In part, these discrepancies might reflect the physicochemical differences between artificial membrane systems and intact NMs as discussed below. Besides, full-length cPLA$_2$ may adsorb tighter to bilayers than its isolated C2-domain owing to additional membrane contacts of its catalytic domain. Since cytoplasmic resting [Ca^{2+}] is estimated to be ~100 nM, our intact nuclei experiments raise the possibility that very strong nuclear stretch, in principle, can replace signal-induced Ca^{2+} transients as cPLA$_2$ activation signal. Under less-extreme conditions, cPLA$_2$ may act as a "coincidence detector" or "AND-gate" for NM-stretch and Ca^{2+} transients. These experiments provide proof of principle that the mechanosensitive features of C2-like domains revealed in our GUV assay likely apply to tension-sensing of full-length proteins on intact cell membranes.

Discussion

Judging from our representative set of membrane-binding domains, we propose that cPLA$_2$-C2 owes its exceptional and conserved stretch-sensitivity to a synergy of at least two mechanosensitive features (*SI Appendix*, Fig. S10). First, stretch increases its Ca^{2+} sensitivity and that of the other tested C2-like domains. Second, stretch permits the insertion of cPLA$_2$-C2 into the hydrophobic membrane core. This distinguishing feature may be restricted to a subgroup of C2-like domains with pronounced, hydrophobic interaction features (i.e., protruding hydrophobic loops or residues), which may have evolved to increase their dynamic mechanosensing range.

We suspect that any membrane-binding motif, naturally occurring or engineered, that exhibits the outlined synergy will be sensitive to membrane tension. Whether membrane insertion and Ca^{2+}-binding must occur within the same domain (as in C2-like domains) or whether interdomain cooperation of these features can also establish mechanosensitivity stands to be seen. Likewise, an intriguing question remains as to whether other chemical ligands in the membrane can substitute for Ca^{2+} in this synergy.

Although our data suggest that cPLA$_2$, in principle, can bind to stretched membranes in the absence of Ca^{2+} signals, it is unclear whether strong nuclear deformation ever occurs

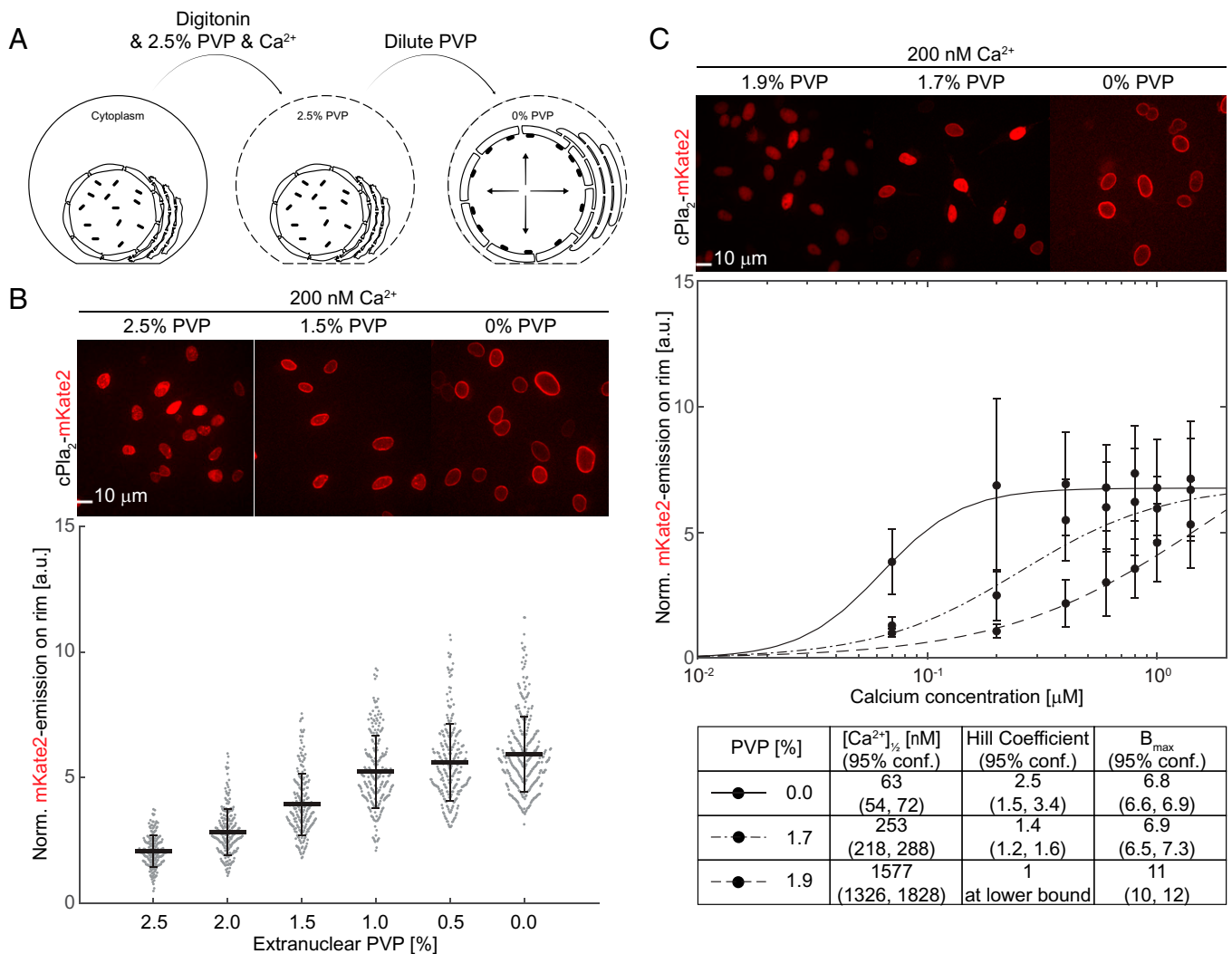| PVP [%]	[Ca^{2+}]$_{\frac{1}{2}}$ [nM] (95% conf.)	Hill Coefficient (95% conf.)	B$_{max}$ (95% conf.)
0.0	63 (54, 72)	2.5 (1.5, 3.4)	6.8 (6.6, 6.9)
1.7	253 (218, 288)	1.4 (1.2, 1.6)	6.9 (6.5, 7.3)
1.9	1577 (1326, 1828)	1 at lower bound	11 (10, 12)

Fig. 3. Membrane tension amplifies cPla$_2$ adsorption to intact NM in A549 cells. (*A*) Experimental scheme. Digitonin was used to permeabilize the plasma membrane. Extranuclear colloid osmotic pressure was adjusted with 360 kDa PVP to control nuclear swelling tension at defined Ca^{2+} concentrations. (*B, Top*) Representative images of *dr* cPla$_2$ located either in the nucleoplasm or bound to the inner NM of A549 cells. (Scale bars, 10 μm.) (*Bottom*) Quantification of cPla$_2$–mKate2 membrane interaction. n > 200 cells per condition. Error bars, SD. [Ca^{2+}] = 200 nM. (*C, Top*) Representative images of cPla$_2$ located either in the nucleoplasm or bound to the inner NM of A549 cells. (Scale bars, 10 μm.) (*Bottom*) Ca^{2+}-isotherms for varying [PVP]. In the table, Hill-fitting of binding curves and binding parameters were determined by nonlinear least-square fitting of data. n >4 0 cells per condition. Error bars, SD. For sample sizes, refer to Dataset S2C.

Shen et al.
A synergy between mechanosensitive calcium- and membrane-binding mediates tension-sensing by C2-like domains

PNAS | 5 of 9
https://doi.org/10.1073/pnas.2112390119

without cyto-/nucleoplasmic Ca^{2+} elevation. Cytoplasmic Ca^{2+} influx from the extracellular space or the ER is directly coupled to cell deformation through mechanosensitive channels like Piezo1 and others (5, 6, 29). In any case, NM-stretch will prime cPLA$_2$ for activation by enabling the enzyme to detect miniscule Ca^{2+} transients. Strong mechanosensitivity, as realized in cPLA$_2$-C2, is not intrinsic to all peripheral membrane-binding motifs, as suggested by our AKT1-PH, Alox12-PLAT, and PKCγ-C2 results.

A popular artificial membrane model for measuring protein–bilayer interactions are highly curved liposomes (e.g., SUVs) generated by membrane sonification or comparable techniques (11, 27, 28). The total curvature of GUVs or nuclei is roughly two orders of magnitude lower than that of SUVs. In "flat" GUV membranes, lipid headgroups are more densely packed than in highly curved membranes of similar lipid composition. Given the larger voids between their headgroups, SUVs are intrinsically primed for adsorption (20, 22, 24, 25, 30, 31). GUV membranes, on the other hand, are basically flat and require stretch to achieve a similar priming. Consistent with this idea, $[Ca^{2+}]_{1/2}$ for cPla$_2$-C2–binding to stretched GUVs ($\sim$1.7 μM) corresponds well to literature measurements on unstretched but curved SUVs (e.g., 3.3 μM) (28), whereas the Ca^{2+} sensitivity on unstretched GUVs is much lower ($[Ca^{2+}]_{1/2} \sim$18 to 36 μM). Likewise, the Ca^{2+} sensitivity of cPla$_2$ interaction with stretched membranes ($[Ca^{2+}]_{1/2} \sim$60 to 90 nM) corresponds well to the Ca^{2+}-sensitivity of PLA$_2$ activity ($[Ca^{2+}]_{1/2} \sim$100 to 200 nM) on sonicated macrophage membranes, which likely are highly curved (27). In the case of A549 cells, the Ca^{2+}-sensitivity of cPla$_2$ interaction with relaxed NM is much lower ($[Ca^{2+}]_{1/2} \sim$1.6 μM). Chemical variables, such as different protein-tagging strategies, recombinant protein quality, and differences in membrane composition may, of course, also contribute to the noted differences between our and literature measurements. Notwithstanding, the above relations and our ALPS experiments together argue that curvature and stretch promote domain adsorption through similar mechanisms (i.e., alteration of lipid-packing), albeit on very different length scales.

By providing a quantitative assay for protein interactions with flat membranes, our GUV method should help to further clarify how physical cues, such as stretch and curvature, regulate peripheral membrane proteins. At the same time, our data establish a quantitative baseline for understanding mechanotransduction through peripheral membrane proteins. We hope that our insights will facilitate the rational design of noninvasive probes that can measure membrane tension in intact cells and tissues.

Methods

Lipids. DPPC, L-α-phosphatidylserine (Brain PS), L-α-phosphatidylinositol-4-phosphate (Brain PI(4)P), DOPC, 1–2-dioleoyl-sn-glycerol (18:1 DOG), 1-oleoyl-2-(6-((4,4-difluoro-1,3-dimethyl-5-(4-methoxyphenyl)-4-bora-3a,4a-diaza-s-indacene-2-propionyl)amino)hexanoyl)-sn-glycero-3-phosphocholine (TopFluor TMR PC), and 1,2-dioleoyl-sn-glycero-3-phosphoethanolamine-N-(lissamine rhodamine B sulfonyl) (18:1 Liss Rhod PE) were purchased from Avanti Polar Lipids. All other chemicals were purchased from MilliporeSigma.

Construction of Expression Vector and Mutagenesis. For bacterial expression, zebrafish cPla$_2$-C2-eGFP-6HIS (zebrafish cPla$_2$ C2 domain spanning amino acids 1 to 131), human cPLA$_2$-C2-eGFP-6HIS (human cPLA$_2$ C2 domain spanning amino acids 1 to 137), Alox5a-PLAT-eGFP-6HIS (zebrafish Alox5a N-terminal PLAT domain spanning amino acids 1 to 118), Alox12-PLAT-eGFP-6HIS (zebrafish Alox12 N-terminal PLAT domain spanning amino acids 1 to 117), PKCγ-C2-eGFP-6HIS (human PKCγ C2 domain spanning amino acids 158 to 289), and AKT1 PH-eGFP-6HIS (human AKT1 PH domain spanning amino acids 1 to 148) were amplified from complementary DNA (cDNA) and cloned into a modified pHAT2 bacterial expression vector backbone. ARFGAP1-ALPS-eGFP and ARFGAP1-ALPS-mCherry (human ARFGAP1-ALPS domain covering amino acids

192 to 304) were cloned into a modified pGEX-6P-1 backbone, leading to N-terminal GST fusion with Human Rhinovirus-3C (HRV-3C) protease cleavage sites.

Double–amino acid mutations of the cPla$_2$-C2-eGFP hydrophobic regions (L32AL33A, L32FL33F, Y90AV91A, and Y90FV91F) and calcium-binding regions (D34RD87R and D34KD87K) were introduced using the QuikChange Lightening Site-Directed Mutagenesis Kit (Agilent Technologies) and the Phusion Site-Directed Mutagenesis Kit (Thermo Fisher Scientific), respectively, with appropriate mutagenesis primers (Table 1) according to the manufacturer's protocol. For mutagenesis of calcium-binding regions, mutations at residue 34 and residue 87 were sequentially introduced to the plasmid.

For mammalian expression, cPla$_2$-mKate2-P2A-eGFP-Alox12 or cPla$_2$-mKate2 were cloned into the pSB/EF-1α/MCS/Puro transposon plasmid as previously described (32). Within this plasmid, an expression cassette containing cPla$_2$-mKate2-P2A-eGFP-Alox12 or cPla$_2$-mKate2 is driven by a constitutive EF-1α promoter along with another expression cassette that encodes a puromycin selection marker under the control of synthetic RPBSA promoter. Both expression cassettes are flanked by inverted terminal repeats that contain transposase recognition sites and allow transposition into host genome when coexpressed with the hyperactive *Sleeping Beauty* transposase.

Recombinant Protein Expression and Purification. The expression and purification of C-terminally tagged C2 or PLAT domains was performed as previously described (4). In brief, the pHAT2 vectors containing the C-terminally tagged C2 or PLAT domains were transformed into *Escherichia coli* BL21 cells (New England Biolabs). Expression was induced by 0.2 mM isopropyl-β-D-thiogalactopyranoside (IPTG) (Promega) in 1 L Luria Bertani (LB) culture supplemented with Ampicillin (100 μg/mL) at optical density (OD)$_{600}$ = 0.5 under vigorous shaking at 250 revolutions per minute (RPM) overnight at 18 °C. Bacteria were centrifuged at 2,600 relative centrifugal force (RCF) for 30 min, pelleted, and frozen at −80 °C. For purification, bacteria were resuspended in 25 mM Hepes (pH =7.4) and 0.1% Triton X-100 with protease inhibitors (cOmplete, ethylenediaminetetraacetic acid-free protease inhibitor mixture, Roche). Sonication was conducted on an ice/water mixture for 7 to 10 min with the following settings: 50% Amplitude, 1-s-on/2-s-off pulses (Thermo Fisher Scientific Sonic Dismembrator Model 500). After sonication and centrifugation at 24,000 RCF for 30 min at 4 °C (Sorvall RC 6 PLUS, Rotor SS-34), the supernatants were collected and incubated with TALON metal affinity resin (Takara) for 3 h under rotation at 4 °C. The affinity resin was rinsed three time with 25 mM Hepes (pH =7.4) and 200 mM potassium chloride (KCl) buffer. For protein elution, the TALON beads were incubated with 2 mL 100 mM imidazole (dissolved in 25 mM Hepes and 200 mM KCl buffer) in disposable gravity columns (Takara) for 10 min, and the flow-through was collected. The eluates were applied to PD10 desalting columns (GE Health), and the collected, fluorescent fractions were concentrated by repeated centrifugation (Amicon Ultra-2 10K Centrifugal Fliter Devices, MilliporeSigma). Protein concentration was determined using the Pierce bicinchoninic acid (BCA) protein assay kit (Thermo Fisher Scientific). Protein purity was determined by sodium dodecyl sulphate–polyacrylamide gel electrophoresis (SDS-PAGE) and Coomassie blue staining. Aliquots were snap frozen in liquid nitrogen and stored at −80 °C.

GST fusions of C-terminally tagged ARFGAP1-ALPS were expressed and purified as previously described (30). The pGEX-6P-1 expression vector harboring tagged ARFGAP1-ALPS was transformed into Rosetta 2 pLySs cells (Novagen). Expression of ARFGAP1-ALPS was induced by 0.2 mM IPTG at 37 °C under vigorous shaking (250 RPM) for 3 h in LB medium supplemented with Ampicillin (100 μg/mL) at OD$_{600}$ = 0.8. After expression, bacteria were resuspended, sonicated, and centrifuged. Supernatants were incubated with Glutathione Sepharose 4B gel beads (Cytiva) overnight at 4 °C. The beads were washed three times in 25 mM Hepes (pH =7.4) and 200 mM KCl buffer afterward. Beads with GST-tagged ARFGAP1-ALPS were incubated with HRV-3C protease (PreScission Protease, Cytiva) in 25 mM Hepes (pH =7.4) and 200 mM KCl overnight at 4 °C to elute ARFGAP1-ALPS. Eluates were concentrated with Amicon Ultra-2 10K centrifugal filter devices. The total protein concentration was determined using the Pierce BCA Protein Assay Kit. Protein purity was determined by SDS-PAGE and Coomassie blue staining. Bands were quantified in Fiji (33). Aliquots were snap frozen in liquid nitrogen and stored at −80 °C.

GUV Preparation. For GUVs composed of DPPC and PS (84% DPPC and 16% Brain PS; 83.5% DPPC, 16% Brain PS and 0.5% TopFluor TMR PC [mol/mol]; 84% DPPC and 16% Brain PS; and 83.5% DPPC, 16% Brain PS, and 0.5% 18:1 Liss Rhod PE), a nylon net hydration method was used. Briefly, 41-μm pore size nylon net filters (MilliporeSigma) were submerged in 25 mL of lipid mixture containing lipids (total amount: 160 μMol) dissolved in 1:1 chloroform/methanol based on the ratios described above. Subsequently, the filter was dried in vacuum for 10 min. In total, 10 mL of warm 500 mM sucrose solution was

Table 1. Mutagenesis primers

Mutagenesis primers	Primer sequence
Y90F V91F Forward	ccaagagtttcatccatgaaaaaattggcatccatcagtgtcacc
Y90F V91F Reverse	ggtgacactgatggatgccaatttttttcatggatgaaactcttgg
Y90A V91A Forward	ccaagagtttcatccatggcagcattggcatccatcagtgtcacc
Y90A V91A Reverse	ggtgacactgatggatgccaatgctgccatggatgaaactcttgg
L32F L33F Forward	ctaaaggagcatttgggggatttcttcgacaccccggac
L32F L33F Reverse	gtccggggtgtcgaagaaatccccaaatgctcctttag
L32A L33A Forward	taagggtccggggtgtccgctgcatccccaaatgctcctttagttacatttt
L32A L33A Reverse	aaaatgtaactaaaggagcatttggggatgcagcggacaccccggacccttta
D34R D87R Forward (D34R)	ggatttattgcgcaccccggacc
D34R D87R Reverse (D34R)	ccaaatgctcctttagttac
D34R D87R Forward (D87R)	gacactgatgcgtgccaattatgtcagt
D34R D87R Reverse (D87R)	acctccaaaacattggattg
D34K D87K Forward (D34K)	ggatttattgaagaccccggacc
D34K D87K Reverse (D34K)	ccaaatgctcctttagttac
D34K D87K Forward (D87K)	gacactgatgaaggccaattatg
D34K D87K Reverse (D87K)	acctccaaaacattggattg

added and incubated with the nylon net filters in tightly closed, amber glass jars (Thermo Fisher Scientific). The jars were incubated for 4 to 6 h at 42 °C. The GUV suspension was diluted with 4 volumes of osmotically matched salt and sucrose solution (107.5 mM KCl, 1 mM MgCl$_2$, 10 mM Hepes, 5 mM ethylene glycol-bis(2-aminoethylether)-N,N,N′,N′-tetraacetic acid (EGTA), and 267 mM sucrose). Vesicles were pelleted at 50 RCF for 1 h and resuspended in the same salt and sucrose solution. For experiments that involved PKCγ-C2, a lipid mixture with increased Brain PS concentration was used: 73.5% DPPC, 26% Brain PS, and 0.5% TopFluor TMR PC dissolved in 1:1 chloroform/methanol (up to a maximum of 30% mol/mol Brain PS concentration above which natural swelling was inhibited). For comparison, gentle hydration by a standard protocol was conducted as described previously (34).

To generate GUVs with alternative lipid compositions (99.5% DOPC and 0.5% 18:1 Liss Rhod PE; 89.5% DOPC, 10% 18:1 DOG, and 0.5% 18:1 Liss Rhod PE; 81.5% DOPC, 18% 18:1 DOG, and 0.5% 18:1 Liss Rhod PE; 99.5% DPPC and 0.5% 18:1 Liss Rhod PE; 100% DPPC; and 83% DPPC, 16.5% Brain PI(4)P, and 0.5% 18:1 Liss Rhod PE), the electroformation technique was performed as previously described (16). Briefly, 0.11 μMol of lipid mixture according to the above described ratios was spread on 30 to 60 Ω indium tin oxide (ITO) coverslips (Structure Probe Inc.supplies) and dried under a N$_2$ stream. ITO coverslips were assembled into an electroformation chamber with 500 mM sucrose solution inside and incubated at 60 °C. The chambers were connected to a function generator (RIGOL DG1022). A sine wave with a frequency of 10.0 Hz and peak-to-peak voltage at 1.41 V was applied for 4 to 6 h followed by a square wave with a frequency of 4.5 Hz and peak-to-peak voltage at 2.12 V for 30 min. After electroformation, GUVs were extracted from the chamber using a gel loading tip. The chamber was washed two times with 500 mM glucose solutions to collect residual GUVs. GUVs were used for experiments within 5 d after preparation.

Recombinant Protein-Binding Experiments. GUV-binding buffers (Table 2) generally contained KCl, EGTA, Hepes, MgCl$_2$, and varying concentrations of CaCl$_2$ and sucrose at pH = 7.4 to 7.5. Free calcium concentration was calibrated by mixing EGTA and CaCl$_2$ as described previously (35).

Glass-bottom, 96-well dishes (Cellvis) were coated with 20 mg/mL bovine serum albumin (BSA) solution for 1 h before the binding experiments to avoid GUV adhesion to the glass. For the experiment depicted in Fig. 1A, GUVs were first shrunk by preincubation in hypertonic solution ($\Delta M_{OSM} = -400$ mOsm) for 1 h. Binding experiments were started by transferring these GUV suspensions (2 to 4 μL) to binding buffer supplemented with 1 μM eGFP-tagged recombinant protein in BSA-coated glass-bottom dishes. For the cPLA$_2$-C2 domains (wild-type and mutants), the free calcium concentration was set to 20 μM. For the C2 and PLAT domains of Alox5a, Alox12, and PKCγ, free calcium concentration was maintained between 200 and 500 μM as indicated. For the AKT1-PH domain, free [Ca^{2+}] was maintained at 500 μM. For ARFGAP1-ALPS, calcium was not included in the solution. Protein binding to GUV membranes was measured at room temperature using a Nikon Eclipse Ti inverted spinning-disk confocal microscope with a Plan Apo 100×/1.45 oil objective or a Plan Apo 40×/0.95 air objective and equipped with a Yokogawa CSU-X1 Spinning Disk unit, an ANDOR iXon ULTRA 897BV EMCCD camera, 488-nm and 561-nm solid-state laser lines (Andor Revolution) and NIS-Elements Software (Nikon). GUV membrane fluorescence was excited at 561

nm and collected through a 620 bandpass emission filter (590 to 650 nm). eGFP fluorescence was excited at 488 nm and collected through a 525 bandpass emission filter (515 to 555 nm). All protein domains were imaged using identical microscope settings. GUVs were allowed to settle in solution for 1 to 2 mins before acquisition. Z-stacks (1.4- to 2-μm steps over 30 μm) were acquired every minute for 30 min.

Competition Experiments. Generally, GUVs with preadsorbed "protein A" were transferred to a buffer containing "protein B" (the competitor) but no "protein A" ± calcium. Specifically, 4 to 6 μL unlabeled GUVs (100% DPPC) were first preincubated with 1 μM fluorescent "protein A" (cPla$_2$-C2-eGFP or ARFGAP1-ALPS-mCherry) in 200 μL hypotonic solution ($\Delta M_{OSM} = 240$ mOsm; 20 μM free Ca^{2+}) for 1 h to allow for membrane adsorption. To initiate competition, ~195 μL of this solution was replaced by 200 μL hypotonic solution with 1 μM "protein B" (ARFGAP1-ALPS-mCherry or cPla$_2$-C2-eGFP). Protein (de-)binding was captured for 1 h using confocal microscopy as described in *Recombinant Protein-Binding Experiments*. To study ARFGAP1-ALPS binding after cPla$_2$-C2 membrane desorption, ~195 μL supernatant of the hypotonic cPla$_2$-C2-eGFP (1 μM) was replaced by 200 hypotonic ARFGAP1-ALPS-mCherry (1 μM) solution without Ca^{2+}. As control, we also monitored ARFGAP1-ALPS-mCherry desorption after transferring GUVs into hypotonic buffer without cPla$_2$-C2-eGFP ($\Delta M_{OSM} = 240$ mOsm; 20 μM free Ca^{2+}).

GUV Membrane Rupture and Protein Desorption. To image GUV rupture, concentrated GUV suspensions (4 to 6 μL) were first incubated for 1 h in hypotonic binding buffers ($\Delta M_{OSM} = 240$ mOsm) containing 1 μM of the indicated domain. Next, the GUVs were transferred to hypotonic binding solution (without proteins). Images were acquired as described in *Recombinant Protein-Binding Experiments*. For fast acquisition, only a single Z-slice of the GUV midsection was acquired per field. Images were acquired every 10 s for 25 min.

Image Processing and Analysis. All image processing and analysis was conducted with the Anaconda distribution of Python (Python ≥ 3.5). Specifically, custom Python 3.7 scripts were written based on the Numpy (36), Scipy (37), Scikit-image (38), Allen Cell Structure Segmenter (39), Cellpose (40) and Napari libraries (41).

To quantify binding of recombinant proteins to GUVs, a semiautomatic Python custom script was developed. Analysis comprised the following steps: First, a line was manually drawn by the user from the center of GUV to the edge to crop a selected GUV from the whole image stack. Afterward, intensity normalization and a three-dimensional Gaussian blur (3-pixel radius) were applied to the cropped GUV stack to remove background noise. A marker-controlled watershed algorithm was used on each slice of the cropped stack to segment the GUV. The slice with largest segmented GUV area was defined as the middle section. Based on the watershed segmentation result, a 3-pixel-wide contour of the GUV was drawn onto the GUV middle section. Lastly, the rim-binding intensity was calculated as the median of all intensities along the contour. To account for fluorescence variabilities across multiple purification batches, raw rim-binding of each domain was normalized by the fluorescence signal of a 1-μM protein solution from same purification batch. To this end, the same confocal settings and contours were used as for the GUV measurements. Both GUV radius and circularity were calculated from the two-

Shen et al.
A synergy between mechanosensitive calcium- and membrane-binding mediates tension-sensing by C2-like domains

PNAS | 7 of 9
https://doi.org/10.1073/pnas.2112390119

Table 2. Buffer compositions

$\Delta\,M_{OSM}$ (Inside – Outside)	Salt concentration	Sucrose concentration
−400 mOsm	107.5 mM KCl, 1 mM MgCl$_2$, 5 mM EGTA, and 10 mM Hepes	667 mM
0 mOsm	107.5 mM KCl, 1 mM MgCl$_2$, 5 mM EGTA, 10 mM Hepes, and varying CaCl$_2$ (0 to 7 mM)	246 to 267 mM
100 mOsm	107.5 mM KCl, 1 mM MgCl$_2$, 5 mM EGTA, and 10 mM Hepes	167 mM
240 mOsm	110.5 to 121 mM KCl, 1 mM MgCl$_2$, 5 mM EGTA, 10 mM Hepes, and varying CaCl$_2$ (0 to 7 mM)	0 mM

dimensional contour of the GUV middle section. Circularity was defined as $1 - \frac{c}{a}$, where c is distance between foci and a is the length of major axis (circularity is equal to 1 when GUV is in circular shape). Detailed explanations and codes are available at https://github.com/joeshen123/GUV-Protein-Binding-Analysis-Program.

An autonomous, custom Python script was used to quantify cPla$_2$-mKate2 binding to intact NMs of A549 or HeLa cells. Maximum-intensity projection images were generated from 3D confocal stacks, followed by a Gaussian blur (3-pixel radius) to remove background noise. A generalist, deep learning-based method (Cellpose) was applied to segment nuclei and generate 3-pixel-wide contours on the rim of each nucleus. cPla$_2$-mKate2 binding to the NM was determined as the median of all intensity values along the contour. To normalize for variabilities due to differential expression of cPla$_2$-mKate2, a binding ratio was calculated by dividing the median intensity value along the NM by the median nucleoplasmic intensity. Detailed explanations and codes are available at https://github.com/joeshen123/Cell-Nucleus-Membrane-Binding-2D.

Equilibrium Binding Experiments. Concentrated GUVs were transferred to binding buffer containing domains at varying concentrations in BSA-coated glass-bottom dishes. GUVs were left in the binding solution for 2 h until protein recruitment approached an equilibrium. Afterward, GUV membrane and protein fluorescence images were simultaneously acquired using a 40× objective as described in *Recombinant Protein-Binding Experiments*. Fluorescence signals on GUV membrane were normalized as described in *Image Processing and Analysis*. For C2-like domains, an apparent dissociation constant K'_d, and maximum binding intensities B_{max} were determined by nonlinear least-square analysis of bound-protein fluorescence (B_{bound}) versus total domain concentration ([Domain]) using a Langmuir-type adsorption isotherm as previously described (42):

$$B_{bound} = B_{max}\left(\frac{[Domain]}{[Domain] + K'_d}\right). \qquad [1]$$

For ARFGAP1-ALPS domains, the apparent dissociation constant K'_d, maximum binding intensity B_{max}, and the apparent Hill coefficient H were determined by nonlinear least-square analysis of bound-protein fluorescence (B_{bound}) versus the total domain concentration ([Domain]) using adsorption isotherm with Hill expansion (43), which fitted the experimental data better than the above equation (assuming no cooperativity):

$$B_{bound} = B_{max}\left(\frac{[Domain]^H}{[Domain]^H + K'^H_d}\right). \qquad [2]$$

To compare the Ca^{2+}-sensitivities of C2-like domains, concentrated GUVs were transferred to binding buffer containing 1-μM domain and varying concentrations of free Ca^{2+} in BSA-coated glass-bottom dishes. GUVs were left in the binding solution for 2 h until protein recruitment approached equilibrium. Images were acquired and analyzed as described in *Recombinant Protein-Binding Experiments* and *Image Processing and Analysis*. The Ca^{2+} concentration required for half-maximal membrane-binding ($[Ca^{2+}]_{\frac{1}{2}}$) was obtained by fitting a Hill equation:

$$B_{bound} = B_{max}\left(\frac{[Ca^{2+}]^H}{[Ca^{2+}]^H + [Ca^{2+}]^H_{\frac{1}{2}}}\right), \qquad [3]$$

where B_{bound}, B_{max}, H, and $[Ca^{2+}]$ refer to the bound-protein fluorescence signal, the maximum protein-binding intensity, the apparent Hill coefficient, and the free Ca^{2+} concentration, respectively. Positive cooperativity ($H \geq 1$) of Ca^{2+}-binding was previously known for C2-like domains (e.g., ref. 28). Hence, we restricted the range of the apparent Hill coefficient to ≥1 for better fitting.

Detailed explanations and MATLAB codes are available at: https://github.com/joeshen123/Shen_PNAS_2021.

Flipper-TR Measurements. Membrane tension Flipper-TR probe was purchased from Cytoskeleton, Inc (CY-SC020). GUVs composed of 99% DPPC + 1%

Flipper-TR in dimethyl sulfoxide (DMSO) were prepared using electroformation. Shortly before starting the experiment, GUVs were added to isotonic solution (ΔM_{OSM} = 0 mOsm, 0 μM free Ca^{2+}) or hypotonic solution (ΔM_{OSM} = 100 mOsm, 0 μM free Ca^{2+}) in BSA-coated glass-bottom wells. For fluorescence lifetime imaging, GUVs were imaged on a Leica SP8 Falcon microscope equipped with Plan Apo 40X/1.1 water lens. GUV membranes were excited with 488 nm laser at 23% laser power and emission sampled with 580- to 625-nm filters. A single Z-plane image was acquired every 25 s for 15 min. Following imaging, the fluorescence decay data were fitted with a double-exponential model to calculate the lifetime for each pixel, and the lifetime image was exported as 512 × 512 single Z-plane image for each time point. For quantification, the fluorescence lifetime for each GUV was calculated by averaging the fluorescence lifetimes on its rim.

Generation of Stable A549 and HeLa Cell Lines. A549 human lung cancer cells (CCL-185, ATCC) were grown in Dulbecco's Modified Eagle's Medium supplemented with 10% fetal bovine serum, 2 mM L-glutamine, and 1% Penicillin–Streptomycin. Lipofectamine 3000 (Thermo Fisher Scientific) was used to transfect A549 cells according to the manufacturer's instructions. To establish stable cell lines expressing cPla$_2$-mKate2-P2A-eGFP-Alox12, A549 cells were transfected with SB100X *Sleeping Beauty* transposase and a pSB/EF-1 α /MCS/Puro transposon vector encoding the genes of interests. A total 48 h after transfection, cells were grown in complete growth medium with 1 μg/mL puromycin for 1 to 2 wk. mKate2 and eGFP double-positive cells were sorted by flow cytometry. The stable HeLa (CCL-2) cell line expressing cPla$_2$-mKate2 had been prepared for a previous publication (4).

cPla$_2$-mKate2 Binding to Intact NM. The following medium ("base medium", BM) was prepared for intact NM-binding experiments: 123 mM KCl, 12 mM NaCl, 1 mM KH$_2$PO$_4$, 1.94 mM MgCl$_2$, 10 mM MOPS, 0.28 mM CaCl$_2$, and 1 mM EGTA/Na$^+$ at pH 7.2 to 7.3. Additional CaCl$_2$ was added into BM to change free-Ca^{2+} concentration as previously described (35). Cell membranes were permeabilized in BM supplemented with 25 μg/mL digitonin (Cayman Chemical) and 2.5% PVP360 (MilliporeSigma) for 15 min as previously described (4). Changing PVP360 concentration allowed to control NM-stretch. To measure NM-binding of cPla$_2$-mKate2 with increasing osmotic stretch, permeabilized cells were washed two times with phosphate-buffered saline (PBS), followed by 2 h incubation in BM supplemented with ~200 nM free Ca^{2+} and a PVP360 concentration ranging from 0 to 2.5%. Z-stacks (1.2-μm steps over 40 μm) were acquired and cPla$_2$-mKate2 membrane-binding quantified as described in *Recombinant Protein-Binding Experiments* and *Image Processing and Analysis*.

To measure the Ca^{2+}-sensitivity of cPla$_2$-mKate2 adsorption to intact NM as a function of NM-tension, CaCl$_2$ was added into BM to vary free [Ca^{2+}] from 0 to 1.4 μM. Different PVP360 concentrations were chosen to compare the effects of increasing NM-stretch: 0%, 1.7% (A549 cells only), and 1.9%. Cells were first permeabilized in BM supplemented with 25 μg/mL digitonin, 2.5% PVP360, and varying free [Ca^{2+}]. After washing two to three times with PBS, the permeabilized cells were incubated in BM supplemented with the indicated concentration of PVP360 (0%, 1.7%, or 1.9%) and free Ca^{2+} (0 to 1.4 μM) for 3 h until binding reached an equilibrium. Z-stacks (1.4 μm z-steps over 30 μm) were acquired, and [Ca^{2+}]$_{1/2}$ was determined by fitting a Hill-type equation as described in *Equilibrium Binding Experiments*.

Structure and Multiple Sequence Alignment. Multiple-protein sequence alignment of the cPLA$_2$-C2 domain was performed using CLUSTALW and Jalview Version 2 (44, 45). Figures of domain structures were generated by PyMOL Molecular Graphics System, Version 2.5.1 Schrödinger, LLC (https://pymol.org/2/).

Statistics. For bar-plot comparisons of fitted coefficients (e.g., [Ca^{2+}]$_{1/2}$, K$_d$'), the error bars denote the 95% CI as calculated by MATLAB's *confint* function. Otherwise, error bars represent the SD. Additional repeats of zebrafish cPla$_2$-C2 equilibrium binding experiments with (DPPC+16%PS) are listed in Dataset S1. Detailed sample sizes for the experiments are provided in Dataset S2 and omitted from the figures for clarity. A two-tailed Students t test assuming unequal variances was used to determine P values using the Microsoft Excel t test function.

1. H. Harizi, J.-B. Corcuff, N. Gualde, Arachidonic-acid-derived eicosanoids: Roles in biology and immunopathology. *Trends Mol. Med.* **14**, 461–469 (2008).
2. B. Enyedi, S. Kala, T. Nikolich-Zugich, P. Niethammer, Tissue damage detection by osmotic surveillance. *Nat. Cell Biol.* **15**, 1123–1130 (2013).
3. S. C. F. Rawlinson, C. P. D. Wheeler-Jones, L. E. Lanyon, Arachidonic acid for loading induced prostacyclin and prostaglandin E(2) release from osteoblasts and osteocytes is derived from the activities of different forms of phospholipase A(2). *Bone* **27**, 241–247 (2000).
4. B. Enyedi, M. Jelcic, P. Niethammer, The cell nucleus serves as a mechanotransducer of tissue damage-induced inflammation. *Cell* **165**, 1160–1170 (2016).
5. A. J. Lomakin et al., The nucleus acts as a ruler tailoring cell responses to spatial constraints. *Science* **370**, eaba2894 (2020).
6. V. Venturini et al., The nucleus measures shape changes for cellular proprioception to control dynamic cell behavior. *Science* **370**, eaba2644 (2020).
7. N. J. Malmberg, D. R. Van Buskirk, J. J. Falke, Membrane-docking loops of the cPLA2 C2 domain: Detailed structural analysis of the protein-membrane interface via site-directed spin-labeling. *Biochemistry* **42**, 13227–13240 (2003).
8. S. Jaud, D. J. Tobias, J. J. Falke, S. H. White, Self-induced docking site of a deeply embedded peripheral membrane protein. *Biophys. J.* **92**, 517–524 (2007).
9. D. Murray, B. Honig, Electrostatic control of the membrane targeting of C2 domains. *Mol. Cell* **9**, 145–154 (2002).
10. E. A. Nalefski et al., Independent folding and ligand specificity of the C2 calcium-dependent lipid binding domain of cytosolic phospholipase A2. *J. Biol. Chem.* **273**, 1365–1372 (1998).
11. S. Kulkarni, S. Das, C. D. Funk, D. Murray, W. Cho, Molecular basis of the specific subcellular localization of the C2-like domain of 5-lipoxygenase. *J. Biol. Chem.* **277**, 13167–13174 (2002).
12. A. H. Pande, S. Qin, S. A. Tatulian, Membrane fluidity is a key modulator of membrane binding, insertion, and activity of 5-lipoxygenase. *Biophys. J.* **88**, 4084–4094 (2005).
13. S. C. Kohout, S. Corbalán-García, A. Torrecillas, J. C. Goméz-Fernandéz, J. J. Falke, C2 domains of protein kinase C isoforms alpha, beta, and gamma: Activation parameters and cation stoichiometries of the membrane-bound state. *Biochemistry* **41**, 11411–11424 (2002).
14. K. E. Landgraf, N. J. Malmberg, J. J. Falke, Effect of PIP2 binding on the membrane docking geometry of PKC alpha C2 domain: An EPR site-directed spin-labeling and relaxation study. *Biochemistry* **47**, 8301–8316 (2008).
15. C.-L. Lai, K. E. Landgraf, G. A. Voth, J. J. Falke, Membrane docking geometry and target lipid stoichiometry of membrane-bound PKCα C2 domain: A combined molecular dynamics and experimental study. *J. Mol. Biol.* **402**, 301–310 (2010).
16. E. M. Schmid, D. L. Richmond, D. A. Fletcher, Reconstitution of proteins on electroformed giant unilamellar vesicles. *Methods Cell Biol.* **128**, 319–338 (2015).
17. A. Colom et al., A fluorescent membrane tension probe. *Nat. Chem.* **10**, 1118–1125 (2018).
18. A. Melcrová et al., The complex nature of calcium cation interactions with phospholipid bilayers. *Sci. Rep.* **6**, 38035 (2016).
19. A. Magarkar, P. Jurkiewicz, C. Allolio, M. Hof, P. Jungwirth, Increased binding of calcium ions at positively curved phospholipid membranes. *J. Phys. Chem. Lett.* **8**, 518–523 (2017).
20. S. Vanni, H. Hirose, H. Barelli, B. Antonny, R. Gautier, A sub-nanometre view of how membrane curvature and composition modulate lipid packing and protein recruitment. *Nat. Commun.* **5**, 4916 (2014).
21. J. Bigay, B. Antonny, Curvature, lipid packing, and electrostatics of membrane organelles: Defining cellular territories in determining specificity. *Dev. Cell* **23**, 886–895 (2012).
22. F. Campelo, M. M. Kozlov, Sensing membrane stresses by protein insertions. *PLOS Comput. Biol.* **10**, e1003556 (2014).
23. N. S. Hatzakis et al., How curved membranes recruit amphipathic helices and protein anchoring motifs. *Nat. Chem. Biol.* **5**, 835–841 (2009).
24. B. Mesmin et al., Two lipid-packing sensor motifs contribute to the sensitivity of Arf-GAP1 to membrane curvature. *Biochemistry* **46**, 1779–1790 (2007).
25. M. Pinot et al., Feedback between membrane tension, lipid shape and curvature in the formation of packing defects. *BioRxiv* [Preprint] (2018). https://doi.org/10.1101/389627. Accessed 22 December 2021.
26. K. E. Ward, R. Sengupta, J. P. Ropa, S. Amiar, R. V. Stahelin, The cytosolic phospholipase A2α N-terminal C2 domain binds and oligomerizes on membranes with positive curvature. *Biomolecules* **10**, 647 (2020).
27. J. Y. Channon, C. C. Leslie, A calcium-dependent mechanism for associating a soluble arachidonoyl-hydrolyzing phospholipase A2 with membrane in the macrophage cell line RAW 264.7. *J. Biol. Chem.* **265**, 5409–5413 (1990).
28. E. A. Nalefski, M. M. Slazas, J. J. Falke, Ca2+-signaling cycle of a membrane-docking C2 domain. *Biochemistry* **36**, 12011–12018 (1997).
29. M. M. Nava et al., Heterochromatin-driven nuclear softening protects the genome against mechanical stress-induced damage. *Cell* **181**, 800–817.e22 (2020).
30. J. Bigay, J.-F. Casella, G. Drin, B. Mesmin, B. Antonny, ArfGAP1 responds to membrane curvature through the folding of a lipid packing sensor motif. *EMBO J.* **24**, 2244–2253 (2005).
31. V. K. Bhatia, N. S. Hatzakis, D. Stamou, A unifying mechanism accounts for sensing of membrane curvature by BAR domains, amphipathic helices and membrane-anchored proteins. *Semin. Cell Dev. Biol.* **21**, 381–390 (2010).
32. E. Kowarz, D. Löscher, R. Marschalek, Optimized Sleeping Beauty transposons rapidly generate stable transgenic cell lines. *Biotechnol. J.* **10**, 647–653 (2015).
33. J. Schindelin et al., Fiji: An open-source platform for biological-image analysis. *Nat. Methods* **9**, 676–682 (2012).
34. D. Needham, T. J. McIntosh, E. Evans, Thermomechanical and transition properties of dimyristoylphosphatidylcholine/cholesterol bilayers. *Biochemistry* **27**, 4668–4673 (1988).
35. T. J. Schoenmakers, G. J. Visser, G. Flik, A. P. Theuvenet, CHELATOR: An improved method for computing metal ion concentrations in physiological solutions. *Biotechniques* **12**, 870–874, 876–879 (1992).
36. S. van der Walt, S. C. Colbert, G. Varoquaux, The NumPy array: A structure for efficient numerical computation. *Comput. Sci. Eng.* **13**, 22–30 (2011).
37. P. Virtanen et al., SciPy 1.0 Contributors, SciPy 1.0: Fundamental algorithms for scientific computing in Python. *Nat. Methods* **17**, 261–272 (2020).
38. S. van der Walt et al., scikit-image contributors, scikit-image: Image processing in Python. *PeerJ* **2**, e453 (2014).
39. J. Chen et al., The Allen Cell Structure Segmenter: A new open source toolkit for segmenting 3D intracellular structures in fluorescence microscopy images. *BioRxiv* [Preprint] (2018). 10.1101/491035.
40. C. Stringer, T. Wang, M. Michaelos, M. Pachitariu, Cellpose: A generalist algorithm for cellular segmentation. *Nat. Methods* **18**, 100–106 (2021).
41. N. Sofroniew et al., napari/napari: 0.3.5. *Zenodo* (2020). https://doi.org/10.5281/zenodo.3900158. Accessed 22 December 2021.
42. B. Sorre et al., Nature of curvature coupling of amphiphysin with membranes depends on its bound density. *Proc. Natl. Acad. Sci. U.S.A.* **109**, 173–178 (2012).
43. P. Drücker, M. Pejic, D. Grill, H.-J. Galla, V. Gerke, Cooperative binding of annexin A2 to cholesterol- and phosphatidylinositol-4,5-bisphosphate-containing bilayers. *Biophys. J.* **107**, 2070–2081 (2014).
44. A. M. Waterhouse, J. B. Procter, D. M. A. Martin, M. Clamp, G. J. Barton, Jalview Version 2–A multiple sequence alignment editor and analysis workbench. *Bioinformatics* **25**, 1189–1191 (2009).
45. J. D. Thompson, D. G. Higgins, T. J. Gibson, CLUSTAL W: Improving the sensitivity of progressive multiple sequence alignment through sequence weighting, position-specific gap penalties and weight matrix choice. *Nucleic Acids Res.* **22**, 4673–4680 (1994).

CELL BIOLOGY

Shen et al.
A synergy between mechanosensitive calcium- and membrane-binding mediates tension-sensing by C2-like domains

PNAS | 9 of 9
https://doi.org/10.1073/pnas.2112390119